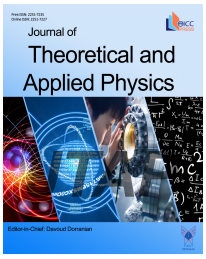

Volume 19, Issue 5, 192546 (1-10)

Journal of Theoretical and Applied Physics (JTAP)

https://doi.org/10.57647/j.jtap.2025.1905.46

Cost effective copper oxide thin layers by highly controlled spray pyrolysis method for optoelectronic devices

Nardjes Randa Hamdaoui[1], Boussaada Salah Eddine[2,*], Younes Hammoudi[2], Lamia Barkat[1], Abdelbacet Khelil[1], Cristina Bogatu Auricia[3], Dana Perniu[3], Anca Duta[3], Younes Mouchaal[1,2]

[1]*LPCMME Lab, Faculty of Exacte and applied Sciences, University Oran 1 Ahmed Ben Bella, Oran, Algeria.*
[2]*Faculty of Exacte Sciences, Mustapha Stambouli Mascara University, Mascara, Algeria.*
[3]*Center for Renewable Energy System and Recycling, R&D Institute of the Transilvania University of Brasov, Brasov, Romania.*

[*]**Corresponding author:** salaheddine.boussaada@univ-mascara.dz

Original Research

Received:
2 June 2025
Revised:
14 August 2025
Accepted:
26 August 2025
Published online:
31 October 2025

Abstract:

Copper Oxide (CuO) thin films were deposited via spray pyrolysis, and the effect of precursor concentration on their structural, morphological, optical, and electrical properties was systematically investigated. X-ray diffraction confirmed a monoclinic crystal structure with optimal crystallinity at 0.06 M, yielding a crystallite size of 25.27 nm. SEM and AFM analyses revealed improved surface uniformity, larger grains, and reduced defects at this concentration. The optimized films exhibited 63% average transmittance in the visible range and an optical bandgap between 1.53 and 2.10 eV. These results demonstrate that cost-effective CuO thin films can achieve properties comparable to those of metal oxides produced by more expensive techniques, positioning them as promising candidates for optoelectronic and photovoltaic applications.

Keywords: CuO; Spray pyrolysis; XRD; Optoelectronic; Figure of merit

1. Introduction

Thin films of metal oxide carry immense significance in the fields of physics, chemistry, and material science. These films find practical use in a multitude of technological applications, based on their specific properties. One such metal oxide, copper oxide, is a p-type semiconductor that has garnered significant attention as a viable material [2]. Low cost, abundance in nature, non-toxicity, and versatility for industrial use, all contribute to its appeal [3]. There are two crystalline forms of copper oxide: Cupric (CuO) and Cuprite (Cu_2O). Cubic Cuprite has a direct band gap that varies between 2.1 and 2.6 electron volts, while monoclinic Cupric has a relatively low, indirect band gap ranging from 1.2 to 1.9 electron volts [4]. These oxides are frequently implemented in various applications, including solar cells and photovoltaic devices [5]. Numerous techniques have been employed to deposit copper oxide thin films, including thermal oxidation [6], Sol-gel [7], Evaporation [8], Electro-deposition [9], Spray pyrolysis [10, 11], and Reactive sputtering [12]. Amount this method, spray pyrolysis stands out as a cost-effective, straightforward, and atmospheric-pressure approach that can cover large surface areas utilizing modest equipment [13]. The impact of copper oxide thin film properties is highly dependent on the composition, concentration, and deposition technique [14, 15]. Structural, electrical, optical, and morphological properties are all influenced by the solution composition and concentration [16]. Similarly, the physical properties of the thin films are affected by the deposition technique and conditions [17]. Therefore, researchers have invested

significant effort in studying and optimizing the deposition parameters to produce copper oxide thin films with the desired properties for specific applications.
This study focuses on the synthesis of CuO thin films using the Spray Pyrolysis Deposition (SPD) technique, with particular emphasis on the effect of precursor concentration on the films' morphological, structural, and optoelectronic properties. The objective is to optimize the composition of the precursor solution to produce thin films that offer an optimal balance between high electrical conductivity and excellent optical transmittance, while ensuring suitable surface morphology. Through this approach, we aim to enhance the performance of CuO-based layers for potential applications in optoelectronic devices.

2. Experimental details

2.1 Deposition parameters

In this study, transparent thin films of copper (II) oxide (CuO) were deposited on glass substrates using a home-made spray pyrolysis system (figure 1). Prior to deposition, the substrates underwent a rigorous cleaning procedure involving sequential ultrasonic baths in acetone and ethanol to eliminate organic contaminants and surface impurities, followed by ambient air drying. Precursor solutions with varying concentrations (0.04, 0.06, 0.10, 0.14 and 0.80 M) were prepared by dissolving copper (II) chloride dehydrate ($CuCl_2 \cdot 2H_2O$, 170.48 g/mol) in 20 mL of ethanol (C_2H_6O). To avoid precipitation and ensure homogeneity, the solutions were stirred at low speed using a magnetic stirrer at 50 °C for 15 minutes. These precursor solutions were subsequently employed to investigate the influence of concentration on the structural and physicochemical properties of CuO transparent conductive thin films. These deposits were subsequently annealed at 500 °C for a duration of one hour.
The deposition parameters of the studied films are collated in Table 1.

2.2 Films characterization

To characterize the structural properties, a Bruker D8 system with CuKα radiation ($\lambda = 0.154056$ nm) was used for XRD analysis. The diffractometer's reflection was captured at room temperature, with the 2θ value ranging from $5 - 80°$.
The Hitachi S-3400N SEM microscope was utilized to examine the morphology of the film. Additionally, an EDX detector was integrated with the equipment for elemental analysis purposes.
Using a RAYLEIGH UV-2601 spectrophotometer, measurements were taken to determine the optical transmittance within the $300 - 1100$ nm range. The optical band gaps were then estimated based on the data obtained from fitting the optical transmittance values.
Carriers' concentration, mobility, and electrical conductivity were ascertained by conducting electrical characteristic tests using a Hall effects measurement system under stable room temperature.
Atomic force microscopy using the NT-MDT BL222RNTE was utilized to analyze surface morphology and roughness. The scan size covered 5×5 µm^2.

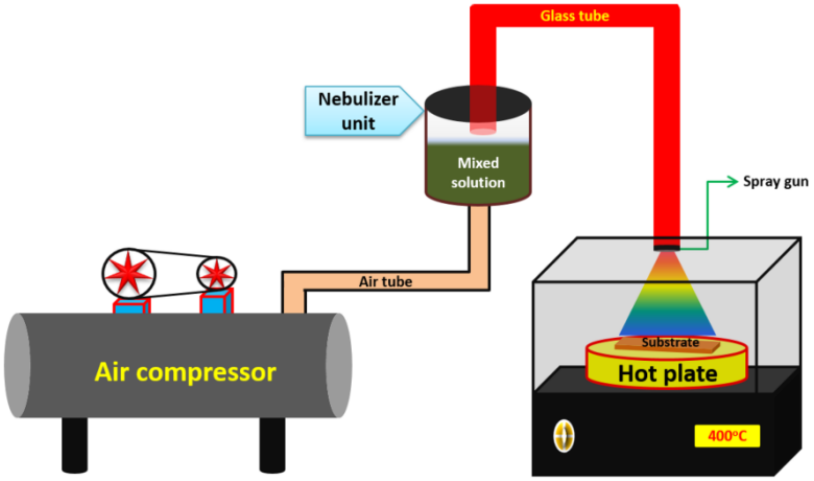

Figure 1. Schematic diagram of nebulizer Spray pyrolysis technique [1].

Table 1. Parameters of deposition of CuO thin films.

Deposition parameters	Values
Distance substrate-nozzle	27 cm
Substrate heating	300 °C
Compressed Air	1.5 bar
Number of cycles	7 times
Annealing temperature	500 °C
Annealing time	1h

3. Results and discussion

3.1 Structural properties

Figure 2 presents the X-ray diffraction (XRD) pattern of CuO thin films. The XRD analysis reveals distinct peaks at 2θ values of 32.46°, 35.51°, 38.70°, 48.80°, 53.50°, 58.21°, 61.58°, 64.60°, 66.29°, 68.01°, 72.37°, and 75.20°, which correspond to the (110), ($\bar{1}11$), (111), ($\bar{2}02$), (020), (202), ($\bar{1}13$), (022), ($\bar{3}11$), (220), (311), and (004) crystal planes, respectively [18, 19]. The identified diffraction planes confirm the monoclinic crystal structure of CuO (space group C2/c), in strong agreement with the standard JCPDS card number 05-0661 [20].

The 2θ value of 35.52° and 38.68° reveal the prominence of the ($\bar{1}11$) and (111) atomic planes respectively in the CuO phase. It can be concluded that the CuO films acquired a monoclinic structure, with a preference for orientation perpendicular to the ($\bar{1}11$) axis. Also a peak located at 2θ value 77.53 corresponding to atomic plan (222) and to cubic Cu_2O plan , this indicates that a part of the deposited CuO films have a cubic structure. Parameters of both observed copper oxide compounds are summarized in (Table 2).

Comparison of the X-ray diffraction patterns of thin films deposited at various concentrations reveals that those prepared at lower concentrations (0.04, 0.06, and 0.1 M) exhibit a higher crystal density. In contrast, films obtained from higher concentrations (0.14 and 0.8 M) display significantly lower crystallinity.

Table 3 shows the films with the highest intensity corresponding to a concentration of 0.06 mol, indicating superior crystallinity compared to the other samples. The cause can be attributed to the fact that lower precursor concentrations promote thin film growth with oxygen saturation, which leads to homogeneous structures with excellent crystallinity [21, 22]. Conversely, high deposition concentrations result in layer by layer or aggregate shaped (metallic Cu and CuO) thin films, in stark contrast to other concentrations where oxygen deficiency causes a stress effect on the structures, subsequently affecting their crystallinity [23, 24].

The lattice parameters $a \neq b \neq c$, $\alpha = \gamma = 90° \neq \beta$ and as well as the unit cell volume "V" of the monoclinic structure are calculated based on the prominent principal peaks of the ($\bar{1}11$) and (111) planes using the following equation [25]:

$$\frac{1}{d^2} = \frac{1}{\sin^2\beta}\left(\frac{h^2}{a^2} + \frac{k^2\sin^2\beta}{b^2} + \frac{l^2}{c^2} + \frac{2hl\cos\beta}{ac}\right) \quad (1)$$

$$V = a \times b \times c \times \sin(\beta) \quad (2)$$

where d represents the inter-planar spacing and (hkl) are the corresponding Miller indices. The results indicate that the lattice parameters and Cell volume (V) of the CuO films obtained from the experiment are consistent with the standard values reported in the JCPDS database for CuO (JCPDS No. 80–1917).

Moreover, revealed the average crystallite size (D) of the CuO thin films' calculated using the Scherrer's relation [26]:

$$D = \frac{0.94\lambda}{\beta\cos\theta} \quad (3)$$

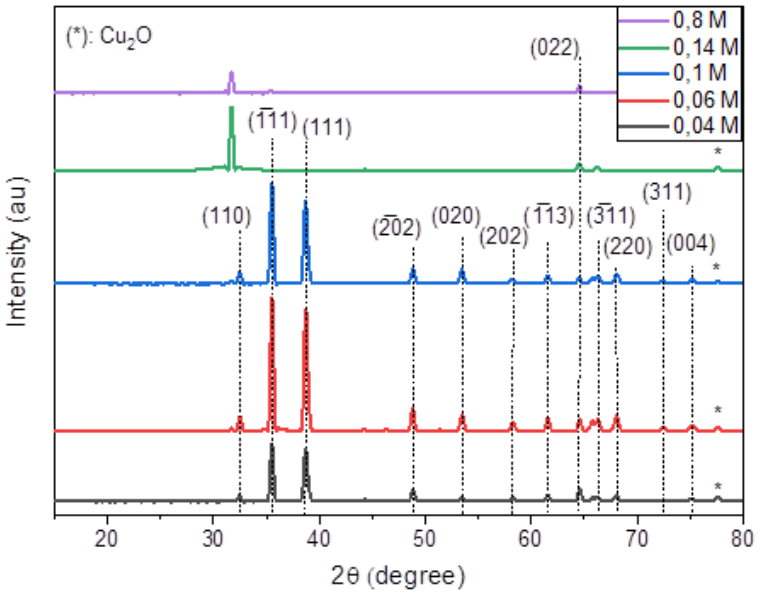

Figure 2. XRD spectra of CuO thin films deposited with different precursor concentration.

Table 2. Crystalline structure of CuO thin films.

Name of phase	Crystal system	Formula	Space group	Volume	Density
Tenorite	monoclinic	CuO	C2/c	81.01	6.505
Cuprite	cubic	Cu_2O	Pn-3m	76.87	6.140

Table 3. Crystallinity and particles size of CuO thin films.

Samples	2θ(°)	(*hkl*)	2θ	Intensity (a.u)	FWHM (°)	Lattice parameters			Cell volume	D (nm)	Strain	Dislocation density
						a (Å)	b (Å)	c (Å)	V (Å^3)		($\varepsilon \times 10^{-2}$)	($\delta \times 10^{14}$ line/m^2)
0,04 M	35,51	($\bar{1}1\bar{1}$)	35,51	391.05	0,34	4,6837	3,4226	5,1320	81,08	24,534	8,0951	16,61
	38,71	(111)	38,71	426.39	0,42	-	-	-	-	20,048	9,9066	24,88
0,06 M	35,52	($\bar{1}1\bar{1}$)	35,52	888,53	0,33	4,6837	3,4226	5,1309	80,99	25,278	7,8568	15,64
	38,72	(111)	38,72	930,19	0,38	-	-	-	-	22,159	8,9628	20,36
0,1 M	35,50	($\bar{1}1\bar{1}$)	35,5	686,95	0,34	4,6837	3,4226	5,1340	81,13	24,533	8,0954	16,61
	38,69	(111)	38,69	676,62	0,43	-	-	-	-	19,580	10,143	26,08

where λ is the X-ray wavelength and has a value of 1.54186 Å, θ is the Bragg diffraction angle and β is the full width at half maximum (FWHM). The deformation (ε) and dislocation density (δ) of the produced thin films were calculated using the following equations [27, 28]:

$$\varepsilon = \frac{\beta \cos\theta}{4} \tag{4}$$

$$\delta = \frac{1}{D^2} \tag{5}$$

The calculated lattice parameters, the crystallite size (D_{hkl}) and FHWM for each sample of CuO films are shown in Table 3.

Figure 3 shows the variation in crystallite size, microstrain, and dislocation density of copper oxide thin films as a function of molar concentration, characterized by values of 25.27 nm, 7.85×10^{-2}, and 15.64×10^4 line/m^2, respectively. The results indicate that a molar concentration of 0.06 M, combined with a substrate temperature of 300 °C, gives optimal crystallization in this study.

3.2 Morphological properties

In figure 4 present the images obtained by Scanning Electron Microscope of the Spray Pyrolysis deposited CuO samples. The SEM images clearly reveal the presence of larger crystallites in the samples with lower concentrations (0.04 and 0.06 M). In contrast, the samples with higher concentrations (0.10, 0.14, and 0.80 M) display smaller crystallites, confined within well-defined grain boundaries. These grain size variations observed in the SEM images are consistent with the crystallite size values obtained from X-ray diffraction analysis, as summarized in Table 3.

EDX analysis was performed to investigate the elemental composition of the CuO thin films. The corresponding results are presented in Table 4. The data confirm the expected composition of the samples through the detected presence of copper (Cu) and oxygen (O).

Topographic AFM images in both 2D and 3D formats for different CuO-based samples are presented in figure 5, with a scanned area of 5 × 5 µm^2. The height of the samples ranges from 1.2 µm to approximately 400 nm, indicating surface roughness. The images display irregular peaks and valleys, reflecting heterogeneous growth with grains or clusters of crystals of various sizes. Figure 6 illustrates the relatively smooth surface texture of CuO samples. With increasing concentration, the surface roughness of CuO thin films decreases. At low concentrations 0.04 M, the film exhibits a relatively high roughness 66.4 nm, which can

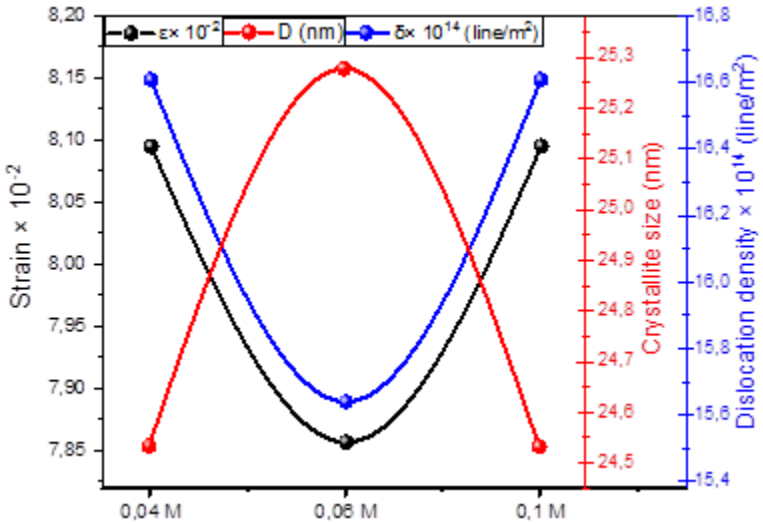

Figure 3. Crystallite size, deformation and dislocation density graph for samples of CuO thin films.

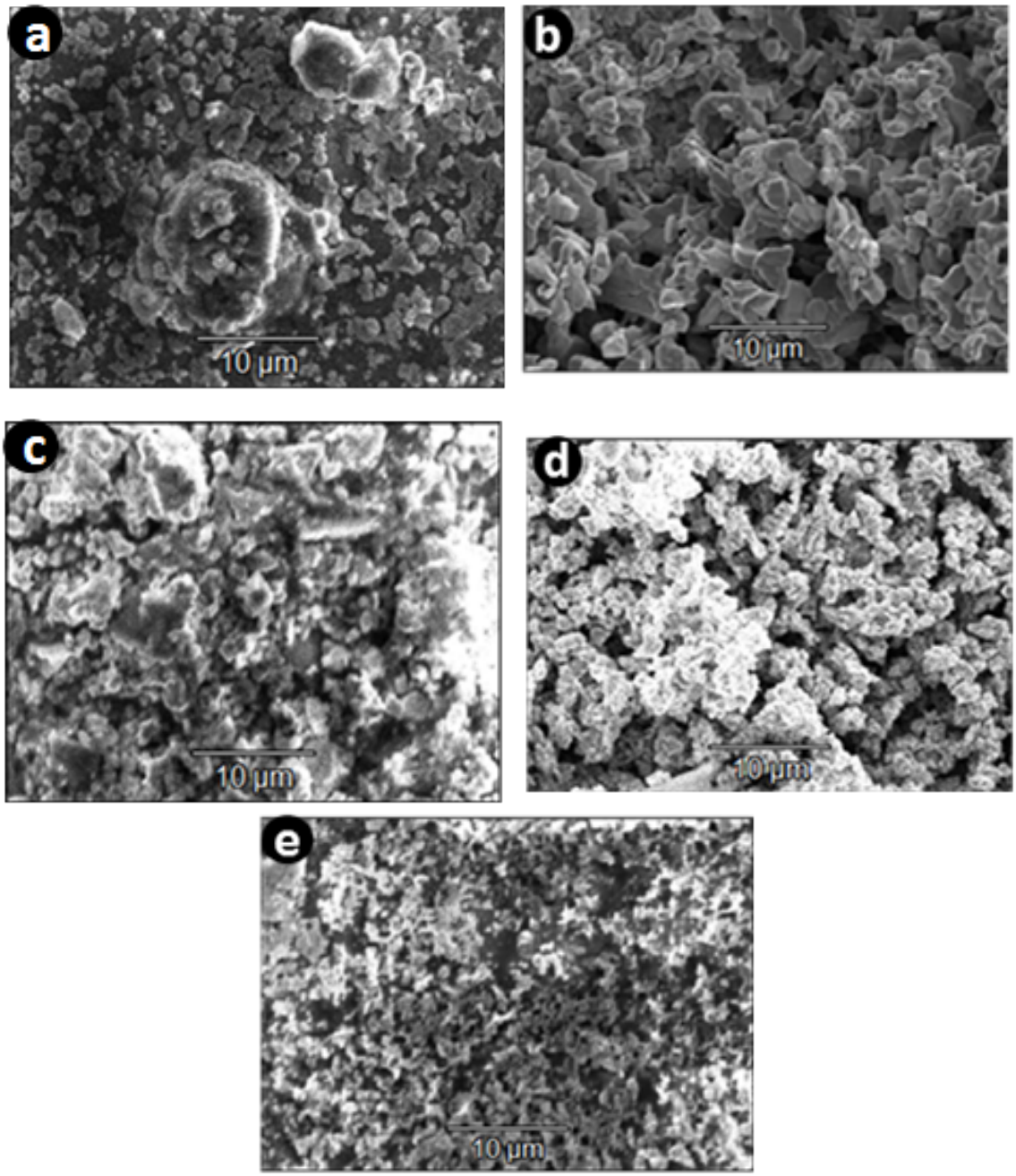

Figure 4. SEM surface image of CuO thin films from different concentration: (a) 0.04 M, (b) 0.06 M, (c) 0.1 M, (d) 0.14 M, and (e) 0.8 M.

be attributed to the presence of larger and irregularly distributed crystallites [29]. This observation is confirmed by the SEM results. As the concentration increases from 0.06 M to 0.80 M, the root mean square roughness gradually decreases, indicating more uniform film growth, smaller grains/crystallites, better compactness, better surface coverage, and reduced surface defects, as shown by the XRD results. At higher concentrations 0.80 M, the film exhibits a relatively smooth surface (with a root mean square roughness of 25.6 nm), resulting in finer and more uniformly distributed grains, minimizing surface height variations.

Table 4. Atomic percentage of Cu and O in samples.

Composition	0.04 M	0.06 M	0.1 M	0.14 M	0.8 M
Cu (At%)	49,43	49,88	49,43	49.72	49.53
O (At%)	50,57	50,12	50,57	50.28	50.47

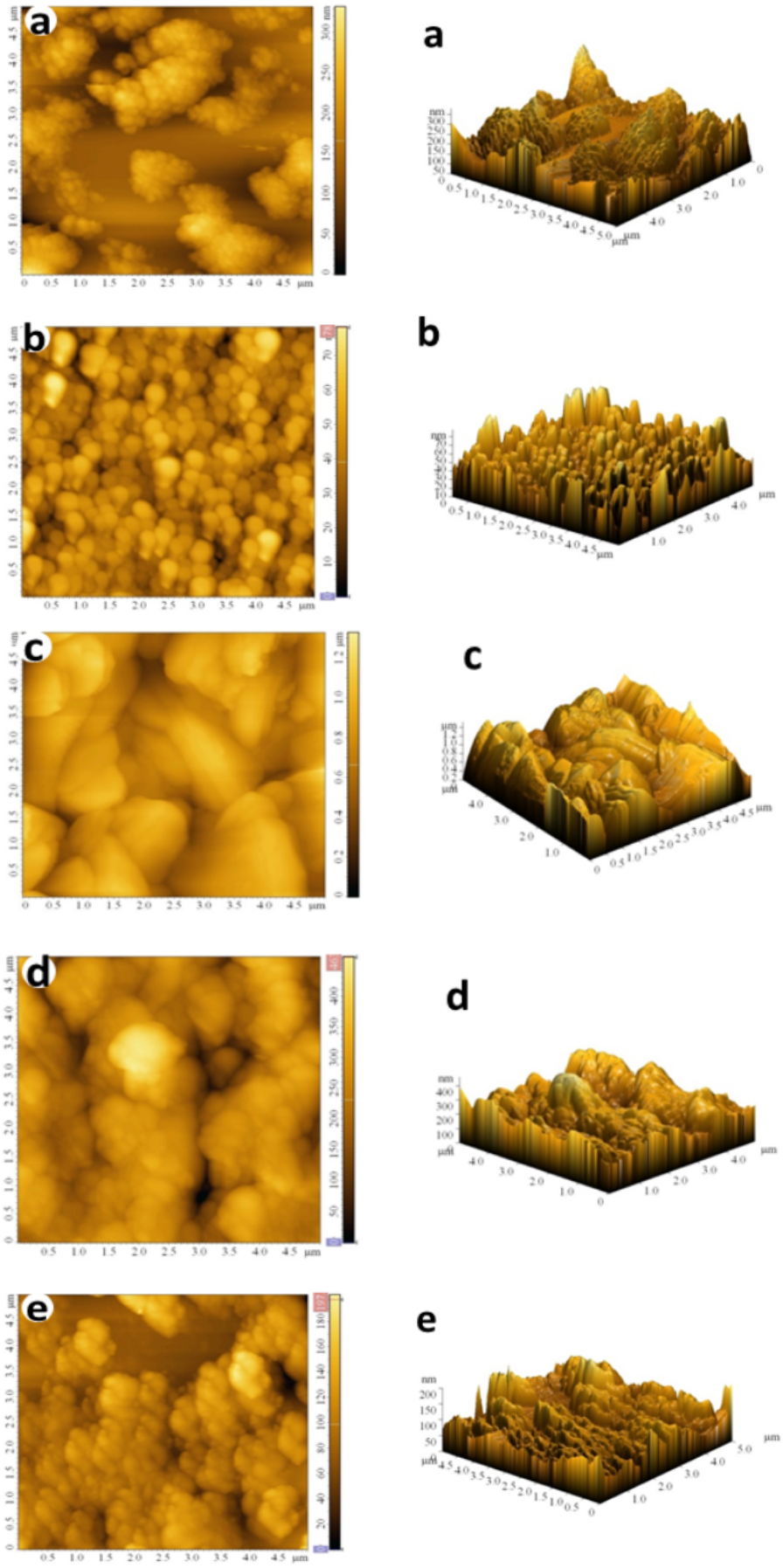

Figure 5. 2D and 3D AFM images of the CuO thin films deposited at (a) 0.04 M, (b) 0.06 M, (c) 0.1 M, (d) 0.14 M, and (e) 0.8 M.

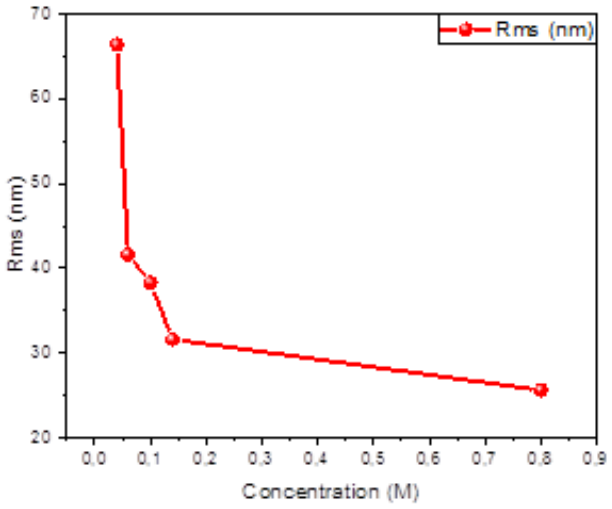

Figure 6. Relatively smooth surface of CuO samples.

3.3 Optical properties

CuO thin films deposited by spray pyrolysis at various concentrations were characterized using UV-Visible spectrophotometry to determine their optical properties. Figure 7 (a) shows the transmittance spectra measured over the wavelength range of 350 to 1100 nm. The 0.06 M thin film exhibits the highest transmittance, around 63%, compared to the films prepared at 0.04, 0.1, 0.14, and 0.8 M, which display lower transmittance. This reduced transmittance in the visible region corresponds to higher absorbance values, as illustrated in figure 7 (b), due to electronic transitions from the valence band to the conduction band. The highest absorbance values are observed at higher precursor concentrations, with a maximum value of 1.5 recorded for the 0.8 M film.

The Tauc relation was used to calculate the optical bandgap energy for the relevant samples [30].

$$(\alpha h\nu)^n = B(h\nu - E_g) \tag{6}$$

where E_g is optical gap energy, α is absorption coefficient, B is constant and $h\nu$ is energy of the incident photon.

We have also used the mathematical formula:

$$E = \frac{hc}{\lambda} \tag{7}$$

where h is Plank's constant, c is the speed of light, and λ is the absorption wavelength.

In figure 8, the variation of the $(\alpha h\nu)^2$ quantity as a function of photon energy $(h\nu)$ is presented. From these curves, the optical bandgap values of CuO thin films at different precursor concentrations were determined and are summarized in Table 5. It is evident that the optical bandgap energy of CuO decreases from 2.10 eV to 1.53 eV as the precursor concentration increases. In this context, copper oxide (CuO) emerges as a simple, cost-effective material with strong absorption in the visible spectrum and a suitable bandgap for photovoltaic devices, offering a promising alternative to rare and expensive materials. As a result, our CuO thin films demonstrate significant potential as hole transport layers (HTL) in perovskite solar cell applications.

3.4 Electrical properties

The electrical properties of the deposited CuO thin films were investigated using the Hall effect technique in a Van der Pauw configuration. Metallic contacts were applied at the four corners of each sample. A constant current was passed between two consecutive contacts (I1-2), while the resulting voltage was measured across the opposing contacts (V4-3).

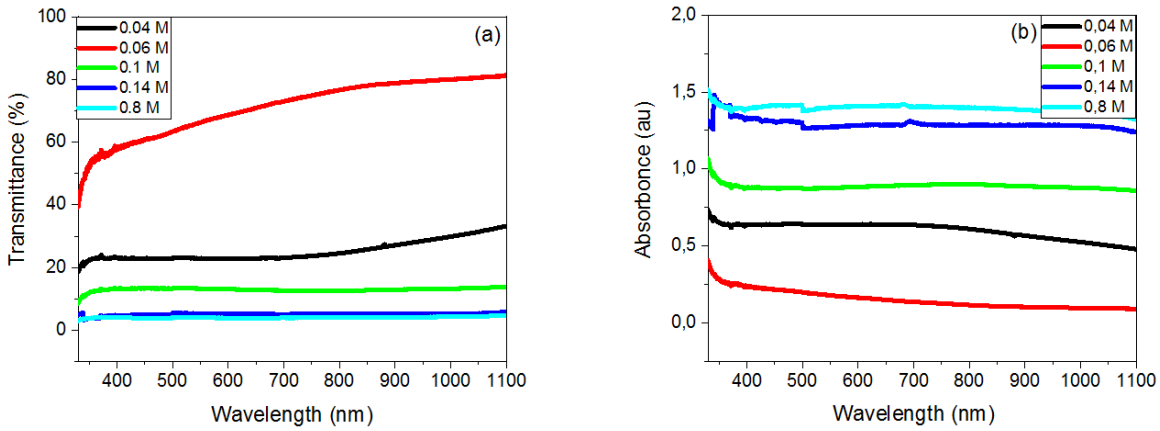

Figure 7. (a) Transmittance and (b) absorbance of CuO thin films spectra obtained at different concentration.

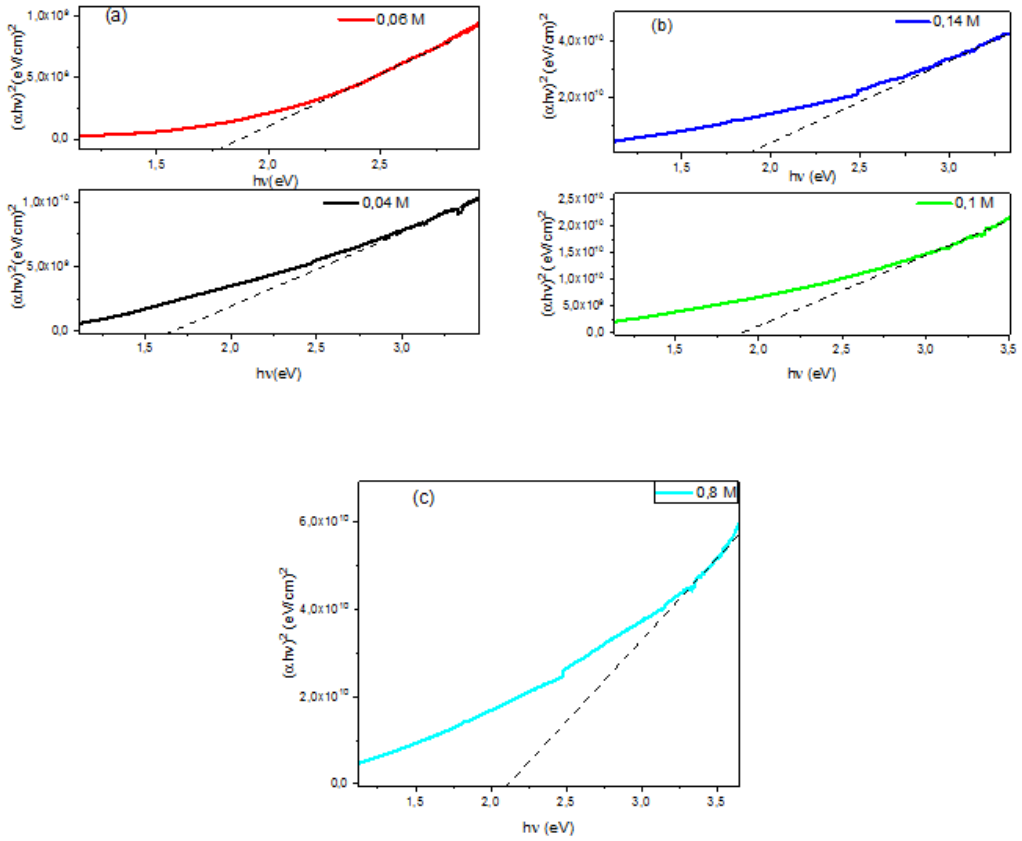

Figure 8. Plot of the $(\alpha h\nu)^2$ curve versus $h\nu$ of thin copper oxide with different concentrations (a) 0.04 and 0.06 M, (b) 0.1 and 0.14 M and (c) 0.8 M.

The electrical parameters of the CuO thin films, measured at various precursor concentrations, are summarized in Table 6. The results clearly demonstrate that precursor concentration has a significant impact on the electrical behavior of the films.

As illustrated in Table 6, both electrical conductivity and carrier mobility exhibit a pronounced increase at a concentration of 0.06 M, reaching values of approximately $9.46 \times 10^3\ \Omega^{-1}\text{m}^{-1}$ and $2.46 \times 10^3\ \text{cm}^2/\text{V}\cdot\text{s}$, respectively. Beyond this concentration, both parameters decrease with further increases in CuO content. This enhancement in conductivity up to 0.06 M can be attributed to the increase in

Table 5. Shows the bandgap of the CuO layers.

Sampels	Average $(300-1100)$	Average $(400-800)$	E_g (eV)
0.04 M	24.87	22.92	1.53
0.06 M	69.45	63.44	1.75
0.10 M	12.96	13.97	1.79
0.14 M	5.13	5.09	1.88
0.80 M	3.99	3.95	2.10

Table 6. Electrical parameters for different CuO thin films.

Samples	Conductivity $\times 10^3\ (\Omega^{-1}\text{m}^{-1})$	Mobility $\times 10^3\ (\text{cm}^2/\text{v}\cdot\text{s})$	Bulk density $\times 10^{19}\ (\text{cm}^{-3})$	Sheet density $\times 10^{14}\ (\text{cm}^{-3})$	ϕ_{TC} Ω^{-1}
0.04 M	2,88	0,40	4,50	4,50	2.6×10^{-3}
0.06 M	9,46	2,46	2,40	2,40	246.95
0.10 M	7.04	1.91	$-2,30$	$-2,30$	9.41×10^{-6}
0.14 M	5,64	1,28	$-2,80$	$-2,80$	7.11×10^{-10}
0.80 M	3.55	0.82	$-2,70$	$-2,70$	3.63×10^{-11}

crystallite size, as confirmed by XRD analysis, and to the higher surface roughness observed in AFM images, both of which contribute to improved charge transport within the films.

To confirm the optimal composition of the deposited CuO structures, we calculated the factor of merit by considering both the electrical conductivity and optical transmittance of the thin films. The Haacke quality factor was employed to evaluate the trade-off between optical and electrical performance [31–33]. The figure of merit, ϕ, proposed by Haacke, is given by the following relation:

$$\phi = T^{10}/R \tag{8}$$

The maximum figure of merit, 246.25 Ω^{-1}, was achieved at a concentration of 0.06 M (Table 6), confirming this composition as the most favorable compromise between optical transparency and electrical conductivity.

4. Conclusion

In this study, we reported the deposition of CuO thin films using the spray pyrolysis technique, with a particular focus on investigating the effect of varying precursor concentrations on their structural, morphological, optical, and electrical properties.

X-ray diffraction analysis revealed distinct diffraction peaks corresponding to the (110) and ($\overline{1}11$) crystallographic planes, confirming the monoclinic crystal structure of the CuO thin films. The crystallite size, microstrain, and dislocation density were determined to be 25.27 nm, 7.85×10^{-2}, and 15.64×10^{-4} lines/m^2, respectively, with optimal crystallization observed at a precursor concentration of 0.06 M. Scanning electron microscopy images clearly demonstrated the formation of larger, well-defined crystals in the 0.06 M samples, while AFM images showed an improved surface morphology with reduced roughness, finer grains, enhanced compactness, and more uniform film coverage, contributing to a decrease in surface defects. By optimizing the precursor concentration, we achieved transparent CuO thin films with remarkable clarity, reaching an average transmittance of 63% in the visible range. Optical measurements revealed an optical bandgap ranging from 1.53 to 2.10 eV, in good agreement with values reported in the literature. These findings suggest that the properties of CuO films are comparable to those of other metal oxides typically produced by more expensive techniques, paving the way for the integration of CuO as a buffer layer or anode material in optoelectronic devices, particularly in solar cell applications.

Funding statement
This work was supported by The Algerian Ministry of Higher Education and Scientific Research (MESRS) and the General Direction of Scientific Research and Scientific Development (DGRSDT).

Authors Contribution
Computational optimisation and computations were carried out by Younes Mouchaal, Nerdjes Randa Hamdaoui and Boussaada Salah Eddine. Investigations on performed solar cells were supported by Cristina Bogatu Auricia, Dana Perniu, Anca Duta and Lmia Barkat data plots and analyses. The main manuscript was written and performed by Nerdjes Randa Hamdaoui, Boussaada Salah Eddine and Younes Hammoudi. The current study was supervised by Younes Mouchaal, Abdelbacet Khelil. The manuscript has been read and reviewed by all authors.

Availability of data and materials
The data that support the findings of this study are available from the corresponding author upon reasonable request.

Conflict of interests
The authors declare that they have no known competing financial interests or personal relationships that could have appeared to influence the work reported in this paper.

References

[1] A. Rohini Devi, A. Jegatha Christy, K. Deva Arun Kumar, S. Valanarasu, M. S. Hamdy, K. S. Al-Namshah, A. M. Alhanash, D. Vikraman, and H.-S. Kim. "Physical properties evaluation of nebulized spray pyrolysis prepared Nd doped ZnO thin films for opto-electronic applications.". *J Mater Sci: Mater Electron*, **30**:7257–7267, 2019. DOI: https://doi.org/10.1007/s10854-019-01039-z.

[2] T. Baran, A. Visibile, M. Busch, X. He, S. Wojtyla, S. Rondinini, A. Minguzzi, and A. Vertova. "Copper oxide-based photocatalysts and photocathodes: Fundamentals and recent advances.". *Molecules*, **26**:7271, 2021. DOI: https://doi.org/10.3390/molecules26237271.

[3] S. Naz, A. Gul, M. Zia, and R. Javed. "Synthesis, biomedical applications, and toxicity of CuO nanoparticles.". *Appl Microbiol Biotechnol*, **107**:1039–1061, 2023. DOI: https://doi.org/10.1007/s00253-023-12364-z.

[4] W.-J. Lee and X.-J. Wang. "Structural, Optical, and Electrical Properties of Copper Oxide Films Grown by the SILAR Method with Post-Annealing.". *Coatings*, **11**:864, 2021. DOI: https://doi.org/10.3390/coatings11070864.

[5] Y. Alajlani, F. Placido, H. O. Chu, R. De Bold, L. Fleming, and D. Gibson. "Characterisation of Cu2O/CuO thin films produced by plasma-assisted DC sputtering for solar cell application.". *Thin Solid Films*, **642**:45–50, 2017. DOI: https://doi.org/10.1016/j.tsf.2017.09.023.

[6] V.-H. Castrejón-Sánchez, A. C. Solís, R. López, C. Encarnación-Gomez, F. M. Morales, O. S. Vargas, J. E. Mastache-Mastache, and G. V. Sánchez. "Thermal oxidation of copper over a broad temperature range: Towards the formation of cupric oxide (CuO).". *Mater. Res. Express*, **6**:075909, 2019. DOI: https://doi.org/10.1088/2053-1591/ab1662.

[7] J. Lillo-Ramiro, J. M. Guerrero-Villalba, M. de L. Mota-González, F. S. A. Tostado, G. Gutiérrez-Heredia, I. Mejía-Silva, and A. C. Castillo. "Optical and microstructural characteristics of CuO thin films by sol gel process and introducing in non-enzymatic glucose biosensor applications.". *Optik*, **229**:166238, 2021. DOI: https://doi.org/10.1016/j.ijleo.2020.166238.

[8] M. F. Al-Kuhaili. "Characterization of copper oxide thin films deposited by the thermal evaporation of cuprous oxide (Cu_2O).". *Vacuum*, **82**:623–629, 2008. DOI: https://doi.org/10.1016/j.vacuum.2007.10.004.

[9] N. M. Rosas-Laverde, A. I. Pruna, J. Cembrero, and D. Busquets-Mataix. "Electrodeposition of ZnO/Cu_2O Heterojunctions on Ni-Mo-P Electroless Coating.". *Coatings*, **10**:935, 2020. DOI: https://doi.org/10.3390/coatings10100935.

[10] D. Naveena, T. Logu, R. Dhanabal, K. Sethuraman, and A. C. Bose. "Comparative study of effective photoabsorber CuO thin films prepared via different precursors using chemical spray pyrolysis for solar cell application.". *J Mater Sci: Mater Electron*, **30**:561–572, 2019.
DOI: https://doi.org/10.1007/s10854-018-0322-4.

[11] S. E. Boussaada, Y. Mouchaal, H. Riane, and A. Khelil. "An investigation of structural, electrical and optical properties of metal free-Zinc Oxide Thin Films Using Spray Pyrolysis Sol-Gel Techniques.". *Egyptian Journal of Chemistry*, 2024.
DOI: https://doi.org/10.21608/ejchem.2024.266541.9265.

[12] A. Rydosz, K. Dyndał, W. Andrysiewicz, D. Grochala, and K. Marszałek. "GLAD Magnetron Sputtered Ultra-Thin Copper Oxide Films for Gas-Sensing Application.". *Coatings*, **10**:378, 2020.
DOI: https://doi.org/10.3390/coatings10040378.

[13] R. M. Pasquarelli, D. S. Ginley, and R. O'Hayre. "Solution processing of transparent conductors: from flask to film.". *Chem. Soc. Rev.*, **40**:5406–5441, 2011.
DOI: https://doi.org/10.1039/C1CS15065K.

[14] A. Rydosz. "The Use of Copper Oxide Thin Films in Gas-Sensing Applications.". *Coatings*, **8**:425, 2018.
DOI: https://doi.org/10.3390/coatings8120425.

[15] M. R. Johan, M. S. M. Suan, N. L. Hawari, and H. A. Ching. "Annealing Effects on the Properties of Copper Oxide Thin Films Prepared by Chemical Deposition.". *International Journal of Electrochemical Science*, **6**:6094–6104, 2001.
DOI: https://doi.org/10.1016/S1452-3981(23)19665-9.

[16] H. Siddiqui, M. R. Parra, and F. Z. Haque. "Optimization of process parameters and its effect on structure and morphology of CuO nanoparticle synthesized via the sol-gel technique.". *J Sol-Gel Sci Technol*, **87**:125–135, 2018.
DOI: https://doi.org/10.1007/s10971-018-4663-5.

[17] D. Prasanth, K. P. Sibin, and H. C. Barshilia. "Optical properties of sputter deposited nanocrystalline CuO thin films.". *Thin Solid Films*, **673**:78–85, 2019.
DOI: https://doi.org/10.1016/j.tsf.2019.01.037.

[18] A. Umar, A. A. Alshahrani, H. Algarni, and R. Kumar. "CuO nanosheets as potential scaffolds for gas sensing applications.". *Sensors and Actuators B: Chemical*, **250**:24–31, 2017.
DOI: https://doi.org/10.1016/j.snb.2017.04.062.

[19] G. M. Raghavendra, J. Jung, D. Kim, and J. Seo. "Chitosan-mediated synthesis of flowery-CuO, and its antibacterial and catalytic properties.". *Carbohydrate Polymers*, **172**:78–84, 2017.
DOI: https://doi.org/10.1016/j.carbpol.2017.04.070.

[20] K. Chen and D. Xue. "Room-Temperature Chemical Transformation Route to CuO Nanowires toward High-Performance Electrode Materials.". *J. Phys. Chem. C*, **117**:22576–22583, 2013.
DOI: https://doi.org/10.1021/jp4081756.

[21] P. Venkateswari, P. Thirunavukkarasu, M. Ramamurthy, M. Balaji, and J. Chandrasekaran. "Optimization and characterization of CuO thin films for P-N junction diode application by JNSP technique.". *Optik*, **140**:476–484, 2017.
DOI: https://doi.org/10.1016/j.ijleo.2017.04.039.

[22] L. Xu, F. Xian, and W. Kuang. "Growth of high quality CuO thin film and investigation of its abnormal luminescence behavior.". *Physica B: Condensed Matter*, **673**:415505, 2024.
DOI: https://doi.org/10.1016/j.physb.2023.415505.

[23] A. Moumen, G. C. W. Kumarage, and E. Comini. "P-Type Metal Oxide Semiconductor Thin Films: Synthesis and Chemical Sensor Applications.". *Sensors*, **22**:1359, 2022.
DOI: https://doi.org/10.3390/s22041359.

[24] R. Rahaman. "Structural, morphological, and opto-electrical characterization of Mn and Co doped CuO thin films.". 2025. URL http://lib.buet.ac.bd:8080/xmlui/handle/123456789/5539.

[25] Y. Bouachiba A. Taabouche A. Bouhank Y. Bellal H. Merabti H. Serrar, A. Bouabellou. "Effect of water and methanol solvents on the properties of CuO thin films deposited by spray pyrolysis". *Thin Solid Films*, **686**:137282, 2019.
DOI: https://doi.org/10.1016/j.tsf.2019.05.001.

[26] R. Zhang, M. Hummelgård, and H. Olin. "A facile one-step method for synthesising a parallelogram-shaped single-crystalline ZnO nanosheet.". *Materials Science and Engineering: B*, **184**:1–6, 2014.
DOI: https://doi.org/10.1016/j.mseb.2013.12.009.

[27] S. M. Mariappan, M. Shkir, T. Alshahrani, V. Elangovan, H. Algarni, and S. AlFaify. "Insight on the optoelectronics and enhanced dielectric properties of strontium decorated PbI2 nanosheets for hot carrier solar cell applications.". *Journal of Alloys and Compounds*, **859**:157762, 2021.
DOI: https://doi.org/10.1016/j.jallcom.2020.157762.

[28] M. Shkir, K. V. Chandekar, A. Khan, T. Alshahrani, A. Mohamed El-Toni, M. A. Sayed, A. K. Singh, A. A. Ansari, M. R. Muthumareeswaran, A. Aldalbahi, R. K. Gupta, and S. AlFaify. "Tailoring the structure-morphology-vibrational-optical-dielectric and electrical characteristics of Ce@NiO NPs produced by facile combustion route for optoelectronics.". *Materials Science in Semiconductor Processing*, **126**:105647, 2021.
DOI: https://doi.org/10.1016/j.mssp.2020.105647.

[29] Y.-T. Sul, C. B. Johansson, S. Petronis, A. Krozer, Y. Jeong, A. Wennerberg, and T. Albrektsson. "Characteristics of the surface oxides on turned and electrochemically oxidized pure titanium implants up to dielectric breakdown: The oxide thickness, micropore configurations, surface roughness, crystal structure and chemical composition.". *Biomaterials*, **23**:491–501, 2002.
DOI: https://doi.org/10.1016/S0142-9612(01)00131-4.

[30] M. K. Hossain, D. P. Samajdar, R. C. Das, A. A. Arnab, Md. F. Rahman, M. H. K. Rubel, Md. R. Islam, H. Bencherif, R. Pandey, J. Madan, and M. K. A. Mohammed. "Design and Simulation of Cs2BiAgI6 Double Perovskite Solar Cells with Different Electron Transport Layers for Efficiency Enhancement". *Energy Fuels*, **37**:3957–3979, 2023.
DOI: https://doi.org/10.1021/acs.energyfuels.3c00181.

[31] G. Haacke. "New figure of merit for transparent conductors.". *Journal of Applied Physics*, **47**:4086–4089, 2008.
DOI: https://doi.org/10.1063/1.323240.

[32] W. Q. Li, S. Y. Ma, Y. F. Li, X. B. Li, C. Y. Wang, X. H. Yang, L. Cheng, Y. Z. Mao, J. Luo, D. J. Gengzang, G. X. Wan, and X. L. Xu. "Preparation of Pr-doped SnO_2 hollow nanofibers by electrospinning method and their gas sensing properties.". *Journal of Alloys and Compounds*, **605**:80–88, 2014.
DOI: https://doi.org/10.1016/j.jallcom.2014.03.182.

[33] S. Maheswari, M. Karunakaran, K. Hariprasad, K. Kasirajan, I. L. Poul Raj, L. B. Chandrasekar, T. Alshahrani, M. Shkir, and S. AlFaify. "Noticeable enhancement in NH_3 sensing performance of nebulizer spray pyrolysis deposited SnO_2 thin films: An effect of Tb doping.". *Superlattices and Microstructures*, **154**:106868, 2021.
DOI: https://doi.org/10.1016/j.spmi.2021.106868.